



HAL
open science

Localised detection of thiophenol with gold nanotriangles highly structured as honeycombs by nonlinear sum frequency generation spectroscopy

G. Barbillon, T. Noblet, B. Busson, A. Tadjeddine, Christophe Humbert

► **To cite this version:**

G. Barbillon, T. Noblet, B. Busson, A. Tadjeddine, Christophe Humbert. Localised detection of thiophenol with gold nanotriangles highly structured as honeycombs by nonlinear sum frequency generation spectroscopy. *Journal of Materials Science*, 2018, 53 (6), pp.4554-4562. 10.1007/s10853-017-1832-9 . hal-03006908

HAL Id: hal-03006908

<https://hal.science/hal-03006908>

Submitted on 16 Nov 2020

HAL is a multi-disciplinary open access archive for the deposit and dissemination of scientific research documents, whether they are published or not. The documents may come from teaching and research institutions in France or abroad, or from public or private research centers.

L'archive ouverte pluridisciplinaire **HAL**, est destinée au dépôt et à la diffusion de documents scientifiques de niveau recherche, publiés ou non, émanant des établissements d'enseignement et de recherche français ou étrangers, des laboratoires publics ou privés.

Localized detection of thiophenol with gold nanotriangles highly structured as honeycombs by nonlinear Sum-Frequency Generation spectroscopy

G. Barbillon · T. Noblet · B. Busson · A. Tadjeddine · C. Humbert

Received: date / Accepted: date

Abstract Gold nanotriangles structured as honeycombs and fabricated by nanosphere lithography on a gold film are functionalized by thiophenol molecules in order to be used as plasmonic sensors in nonlinear optical sum-frequency generation (SFG) spectroscopy. The monitoring and the characterization of the surface optical properties are performed by UV-Visible differential reflectance spectroscopy showing an absorbance maximum located at 540 nm for *p*- and *s*-polarisation beams. SFG spectroscopy proves to be effective for thiophenol detection in *ssp*-polarisation scheme while the molecular SFG signal disappears in *ppp*-configuration due to the strong *s-d* interband contribution of gold. However, in *ssp*-configuration, the vibration modes of thiophenol molecules at 3050 and 3071 cm^{-1} are yet observed thanks to the excitation of a transversal plasmon mode by the incident visible laser beam, whereas they are usually very difficult to distinguish by Surface Enhanced Raman Scattering (SERS) and other vibrational optical probes.

Keywords Gold · Thiophenol · Nanosensors · Plasmons · Sum-Frequency Generation

G. Barbillon
EPF-Ecole d'Ingénieurs, 3 bis rue Lakanal, 92330 Sceaux,
France

T. Noblet, B. Busson, A. Tadjeddine, C. Humbert
Laboratoire de Chimie Physique, CNRS, Univ Paris-Sud,
Université Paris-Saclay, 91405 Orsay, France
Tel.: +33-1-69153290
Fax: +33-1-69153328
E-mail: christophe.humbert@u-psud.fr

1 Introduction

The characterization of surface chemical and electronic properties of nanostructured materials compatible with Surface Enhanced Raman Scattering (SERS) [1] and Polarization Modulation-Infrared Reflectance Absorption Spectroscopy (PM-IRRAS) in applications related to sensors [2] constitutes a real challenge in nonlinear optical spectroscopy [3], especially when performed in biological environment [4,5]. Indeed, in the fabrication of SERS substrates, the goal is to reach submonolayer chemical sensitivity by amplification of the local electric field around metallic nanostructures on which the molecules of interest are grafted. This is obviously made possible thanks to the Localized Surface Plasmon Resonance (LSPR) of specifically designed nanostructures as demonstrated for many years on metals (gold, silver) [6–8]. Another possibility is the creation of a hybrid mode coming from the harmonic coupling of the Surface Plasmon Polaritons (SPP) present in a metallic film with the Bragg waves of an array of metallic nanostructures, so that this hybrid mode can be excited in Kretschmann configuration [9]. Whether by chemical synthesis or different lithographic techniques, the metallic nanostructured surfaces are mandatory for the manufacturing of efficient SERS substrates [10–12]. The lithographic methods are well-adapted to finely control the geometry, to tune the optical properties of nanostructures and to obtain a high reproducibility of enhancement factors (EF) for applications in biosensing. In the case of gold nanostructured surfaces, nonlinear optical sum-frequency generation (SFG) spectroscopy has revealed potential assets in usable EF for samples made of nanopillars (140 nm height, 70 nm diameter) dispersed on metal substrates and prepared by wet chemistry [13]. On non-metallic substrates, the most

emblematic case is illustrated by the study of small spherical nanoparticles of 15 nm diameter obtained by citrate reduction of gold salts and deposited with a surfactant at the air/water interface [14] or grafted on silicon [15,16], glass [17] or quartz [18,19] substrates before their functionalization by probe molecules such as alkane chains [20–22] or aromatic rings [23]. The case of arrays of small gold nanostructures specifically fabricated for high SERS EF was never compared with SFG spectroscopy to the best of our knowledge. In the present work, we address this question by performing the SFG spectroscopy of thiophenol molecules adsorbed on specific SERS substrates composed of gold nanotriangles structured as honeycombs [24]. In principle, since molecular SFG spectroscopy can be seen as the simultaneous combination of anti-Stokes Raman scattering and IR absorption processes, it should be very sensitive to the SERS activity of this kind of interface as already demonstrated in the abovementioned literature, but based on highly dispersed gold nanoparticles on the probed surface. In SFG spectroscopy, the high degree of symmetry of the surface geometry plays a major role in the response and sensitivity of the detected SFG signal. Contrary to what is observed in SERS, the enhancement factor of the local electric field in the SFG process is a necessary but not sufficient condition to enhance the nonlinear optical response of such an interface. In other words, the extinction of the SFG optical response is directly related to the symmetry degree of the interfacial electronic properties: the more centrosymmetric, the greater the extinction of the nonlinear second order process. Despite these strong constraints, we show in this paper that the excitation of a transversal plasmon mode (TM) by a visible wavelength on such interfaces allows the first experimental observation by SFG spectroscopy of two close thiophenol vibration modes in this spectral range.

2 Experimental details

2.1 Fabrication of Gold Nanotriangles by Nanosphere Lithography (NSL)

The fabrication of Au nanotriangles (AuNT) involves six steps: (i) glass substrate cleaning, (ii) electron beam evaporation (EBE) of titanium and gold layers, (iii) drop-coating of colloidal polystyrene beads on gold film, (iv) Au layer deposition by EBE, (v) lift-off process. Firstly, the glass substrates were cleaned with ethanol, acetone, and Piranha solution ((3:1) $\text{H}_2\text{SO}_4/\text{H}_2\text{O}_2$ 30%). Then, we evaporated by EBE a 2 nm titanium layer (adhesion layer) and a gold film (30 nm). The next step was the drop-coating of colloidal bead solutions with a bead

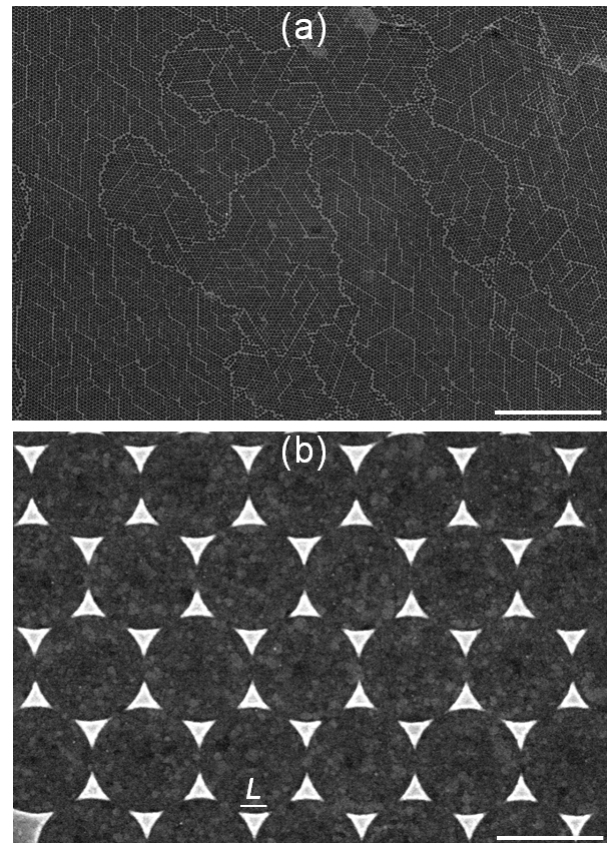


Fig. 1 SEM images of gold nanotriangles on gold film obtained by NSL: (a) on a large surface (scale bar = 15 μm) and (b) on a zoom of some nanotriangles showing $p6mm$ symmetry (scale bar = 500 nm)

diameter of 500 nm (Polysciences GmbH) on the gold film [24,25]. Then, we realized gold layer evaporation (60 nm) by EBE on polystyrene beads. Finally, after a lift-off process in acetone, Au nanotriangles structured in honeycombs on the surface with $p6mm$ symmetry class [26,27] were obtained as displayed in Figure 1. The average length L of nanotriangles is 150 nm. The filling factor [10] of the substrate by the nanotriangles determined by Surface Electron Microscopy (SEM) is 8%, a value similar to the 7.2% deduced from theoretical calculations [26].

2.2 UV-Visible Absorbance Spectroscopy

UV-Visible spectroscopy is performed on a Cary-5000 spectrophotometer (Agilent) for the sample set in reflection geometry with a 55° angle of incidence with respect to the surface normal thanks to a Veemax accessory (Pike Technologies). This angle of incidence is identical to the one used for the visible laser beam in SFG spectroscopy as sketched in Figure 2. Measurements are recorded from 400 to 800 nm with the inci-

dent light either p - or s -polarized in order to compare with the results obtained by SFG spectroscopy. A reference spectrum of the same substrate but without the AuNT is first recorded to extract only the UV-Visible absorbance spectrum of the nanostructured layer by differential measurement.

2.3 Sum-Frequency Generation spectroscopy

Nonlinear optical Sum-Frequency Generation (SFG) spectroscopy [28,29] is performed on a home-made setup as described elsewhere [22]. Briefly, it is based on a pulsed Nd:YVO4 laser source (HighQ laser, 62.5 MHz repetition rate, 7.5 ps pulsewidth, 1064 nm wavelength) acting as a pump, after its passing through two amplifiers, for the two optical parametric oscillators (OPO) tunable in the infrared (LiNbO3, 2.5-4 μm) and the visible (BBO, 420-710 nm) spectral ranges, respectively. In the visible case, the UV pump wavelength (355 nm) was obtained by partial parametric conversion of the near-IR source by second harmonic generation (SHG) through a BBO crystal (532 nm) followed by the mixing (collinear bulk SFG) of the two resulting beams (1064 and 532 nm) through a LBO crystal. As sketched in Figure 2, in order to obtain the SFG signal from the samples, the IR and visible beams are sent to the same point of the surface where they overlap spatially and temporally with either a ppp - or ssp -polarisation configuration for the SFG, visible and IR beams, respectively. The SFG photons are then collected by photomultipliers after spatial and spectral filtering through a monochromator. The SFG contribution of the sample is normalized by the SFG signal of a reference ZnS crystal collected in the same conditions in order to compensate for fluctuations of the laser powers.

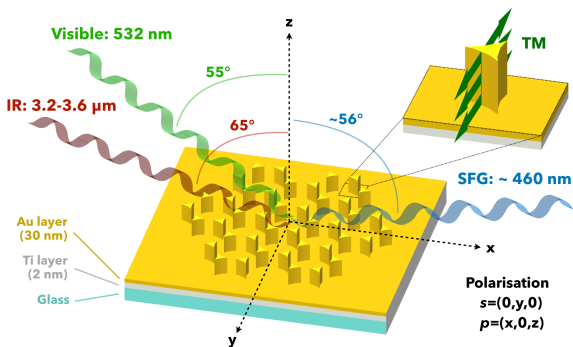


Fig. 2 Scheme of the interface probed by SFG spectroscopy. The SFG, visible and IR beams are travelling in the same incidence xz plane. The incidence angle of 55° for the visible laser beam is the same as the one used in UV-Visible absorbance spectroscopy. The zoom on a nanotriangle illustrates the transversal plasmon mode (TM) excited in ssp -polarisation

3 Results

3.1 UV-Visible absorbance spectra

As depicted in Figure 3, we observe on our sample that the surface absorbance in p -polarisation is stronger than that in s -polarisation to the tune of almost a factor of three. The absorbance spectra exhibit a maximum located at 540 nm for both s - and p -polarisations. In s -polarisation, this peak corresponds to the transversal localized surface plasmon resonance (TM, lateral sides, see zoom in Figure 2) for nanostructured objects relatively similar to the case of gold nanopillars deposited above a gold interface [13]. In p -polarisation,

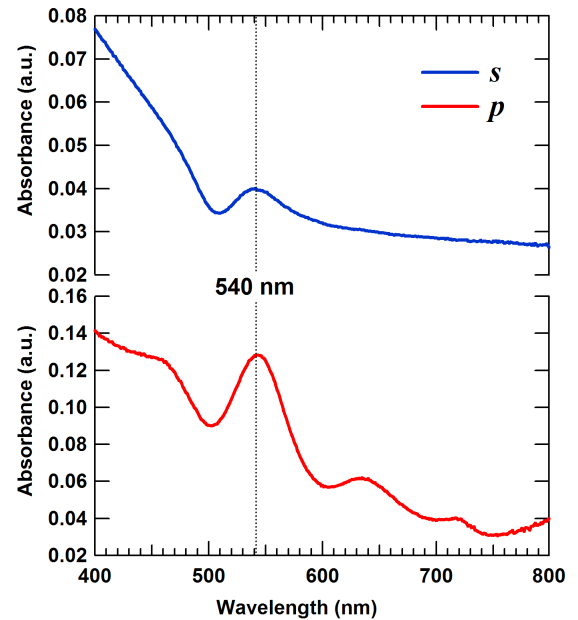


Fig. 3 UV-Visible absorbance spectra of the AuNT/Au/Ti/Glass samples with the light beam having 55° incidence angle for s (up) and p (down) polarisations. The reference sample used to obtain the differential measurement is the Au/Ti/Glass substrate.

the absorbance maximum observed at 540 nm can be attributed to the vertical plasmon mode [30]. Furthermore, in p -polarisation, two surface plasmon modes are observed at 640 and 720 nm, respectively. They can be attributed to the grating resonances coupled to antisymmetric surface plasmon polariton (SPP) modes. In s -polarisation, no plasmon resonance coming from these SPP modes is observed in the 600-800 nm spectral range. This is explained by the fact that SPP modes are only excited by a p -polarized light.

3.2 SFG measurements

Figure 4 shows the SFG spectra of the sample in both *ssp*- and *ppp*-polarisation configurations, respectively. At first sight, we observe the vibrational fingerprint of thiophenol molecules adsorbed on the sample only in *ssp*-configuration. The vibration mode is located at 3071 cm^{-1} as deduced from the fitting procedure of the data explained elsewhere [15]. As it will be detailed further in Figure 5, it corresponds in fact to the combination of two close vibration modes as referenced and calculated from DFT calculations on gold clusters [31]. They are related to the stretching of the CH bonds of the aromatic ring. No vibrational feature is observed in *ppp*-configuration. Nevertheless, there exists a strong flat contribution of one order of magnitude greater than in the *ssp* case. Indeed, a quick look at Figure 4 shows that the average SFG intensity observed in *s*-polarisation is 50 times lower than in *p*-polarisation. The SFG signal of the gold film and AuNT is usually

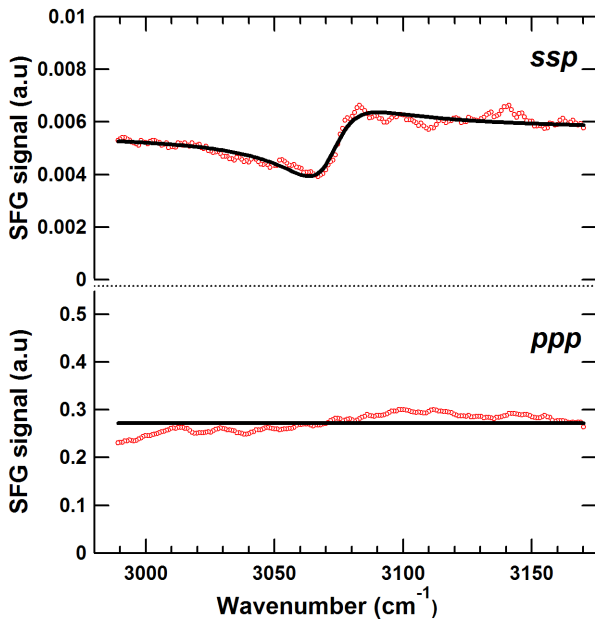


Fig. 4 SFG spectra of the AuNT/Au/Ti/Glass sample in *ssp* (up) and *ppp* (down) polarization configuration for an incident visible laser beam wavelength of 532 nm. In both cases, the average power delivered on the sample is 5 mW. The line is a fit to the SFG data as detailed in the text.

called the non-resonant part (see equation 2) with respect to the IR wavelength because it is related to the electronic properties of the substrate. In the present case, it comes from the metal *s-d* interband transitions as explained in the literature on the subject for flat gold surfaces [32–35]. Indeed, the glass substrate and the Ti layer do not have any SFG activity in the probed spec-

tral range. The SFG intensity is modelled by [36]:

$$I_{\text{SFG}} = \frac{8\pi^3 \omega_{\text{SFG}}^2 \sec^2 \theta_{\text{SFG}}}{c^3 n_1(\omega_{\text{SFG}}) n_1(\omega_{\text{IR}}) n_1(\omega_{\text{VIS}})} \left\| \chi_{\text{eff}}^{(2)} \right\|^2 I_{\text{IR}} I_{\text{VIS}} \quad (1)$$

with I_{IR} and I_{VIS} the intensities of the incident IR and visible laser beams, respectively. ω_{IR} , ω_{VIS} and ω_{SFG} are the IR, visible and SFG frequencies of the three laser beams involved in the nonlinear process while θ_{SFG} is the angle of incidence of the outgoing beam as sketched in Figure 2. $n_1(\omega)$ is the refractive index of the upper medium at frequency ω , i.e. the ambient air in the present case. $\chi_{\text{eff}}^{(2)}$ is the effective nonlinear second order susceptibility of the probed interface, which includes Fresnel factors and microscopic local-field corrections to the molecular nonlinear second order susceptibilities $\chi_{\text{ijk}}^{(2)}$. The experimental SFG nonlinear susceptibility of an interface is generally fitted by [37]:

$$\chi_{\text{eff}}^{(2)} = |C| e^{i\phi} + \sum_{n=1,2,\dots} \frac{|a_n| e^{i\varphi_n}}{\omega_{\text{IR}} - \omega_n + i\Gamma_n} \quad (2)$$

where the first complex term is the above-mentioned non-resonant (NR) contribution related to the gold optical activity of amplitude C . The sum over Lorentzian oscillators describes the vibration modes of thiophenol. For instance, at a first glance in Figure 4, it seems one should consider only one vibration mode characterised by its frequency ω and damping constant Γ , respectively. The amplitude a is a linear combination of products of the components of the IR transition dipole moment and Raman polarizability tensor while the phase shift $\phi - \varphi$ between the NR and resonant contributions explains the interference feature in the SFG signal. If one vibration mode is considered, ϕ can therefore be set to zero to fix a reference. In these conditions, the fitting parameters of the SFG data in *ssp*- and *ppp*-polarisations configuration are given in Table 1. In *ppp*-configuration, only the NR contribution of the substrate to the SFG signal is clearly evidenced. Nevertheless, it is worth noting that the parameter extracted from the fit is twice as large as expected [23], which is in fact the

Table 1 Fitting parameters of the SFG data in *ssp*- and *ppp*-configurations (Thiophenol/AuNT/Au/Ti/Glass) for one molecular vibration mode.

Parameters	<i>ssp</i>	<i>ppp</i>
$ C $	0.0749	0.5217
ϕ ($^\circ$)	28	0
a	0.2115	-
ω (cm^{-1})	3071.73 (± 3)	-
Γ (cm^{-1})	12.39	-

indication of the presence of the two abovementioned thiophenol vibration modes located at 3071 and 3050 cm^{-1} , and named σ and ϵ , respectively [31]. Their optical responses strongly interfere between each other and with the specific substrate covered with AuNT, so that they cannot be decoupled directly. Indeed, it has been shown that there exist equivalent sets of parameters giving the same SFG spectrum for a given experimental SFG curve [37]. In this way, the best fit depicted in Figure 5 relies on physical hypotheses described hereafter and based on the previous literature on the subject. By

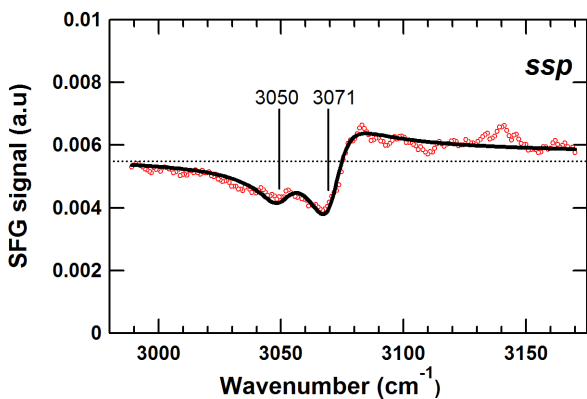


Fig. 5 SFG spectra of the AuNT/Au/Ti/Glass sample in *ssp*-polarisation configuration for an incident visible laser beam wavelength of 532 nm. The average power delivered on the sample is 5 mW. The line is a fit to the SFG data as detailed in the text.

setting the damping constants to 7.5 cm^{-1} [23], we obtain the others parameters after the fitting procedure as depicted in Table 2. It is worth noting that it leads to a solution where the two vibration modes have the same null phase, which is commonly used in the SFG fitting procedures. Moreover, the experimental frequency resolution of the infrared OPO is 3 cm^{-1} as noted in parentheses in Tables 1 and 2, so that our SFG setup is able to discriminate the two vibration modes. These two vibration modes (σ and ϵ) are those with the highest IR and Raman activities when adsorbed on gold clusters as shown by DFT calculations [31], which, with their respective frequencies, is in accordance to the fact that the SFG response of molecules is sensitive to the mixing of their IR and Raman cross-sections. This is why their detection is made feasible by SFG spectroscopy in our experimental configuration. It is also worth noting that their identical absolute phase ($\varphi_1 = \varphi_2 = 0$) is reflected in their same Fano-like spectral shapes.

Table 2 Fitting parameters of the SFG data in *ssp*-configuration (Thiophenol/AuNT/Au/Ti/Glass) for two molecular vibration modes.

Parameters	Non-resonant
$ C $	0.0753
ϕ ($^\circ$)	41.35
Parameters	Mode σ
a_1	0.2115
ω_1 (cm^{-1})	3071.22 (± 3)
Γ_1 (cm^{-1})	7.5
φ_1 ($^\circ$)	0
Parameters	Mode ϵ
a_2	0.05179
ω_2 (cm^{-1})	3050.46 (± 3)
Γ_2 (cm^{-1})	7.5
φ_2 ($^\circ$)	0

4 Discussion

In both polarisation configurations, the dominant contribution to the SFG signal comes from the gold film and triangles. Nevertheless, no thiophenol vibration mode is observed in *ppp*-polarization. It is a different behaviour from what we showed in previous work on a flat Au(111) surface: the SFG spectra of thiophenol are dip-shaped and only one weak vibration mode could emerge in *ppp*-polarization [16]. Although there should be an SFG response coming from thiophenol molecules adsorbed on the gold film between the triangles or adsorbed directly on them, it is clearly masked by the strong *s-d* interband electronic transition of gold in the *z*-direction normal to the surface [32–35]. Moreover, the extinction of the nonlinear second order response of molecules adsorbed on the interface is strongly marked within our nanostructures (*p6mm* symmetry class). Indeed, the SFG signal sensitivity depends on the orientation of the adsorbed molecules (here thiophenol) [38–40]. Thereby, despite the *p6mm* symmetry class of the honeycomb structures, we still detect thiophenol molecules, localized close to the triangle walls in *ssp*-polarisation configuration. More precisely, we distinguish two vibration modes of the molecules. Indeed, the transversal plasmon mode is excited by the contributions of the incident electric field on the triangle walls and the reflected electric field coming from the gold film. Therefore, at a specific height of the triangles walls, the total electric field corresponds to the sum of the incident and reflected electric field contributions, which have a relative phase depending on the distance to the interface [13]. As the SFG emission depends on the total electric field, the SFG amplitude in *ssp*-polarisation

configuration is higher along the triangle height. It is worth noting that these two vibrations were not or weakly observed in the literature [41,42]. Indeed, Wan et al observed only the vibration mode σ at 3060 cm^{-1} on Au(111) surface [31,41] by Surface-Enhanced Infrared Absorption spectroscopy (SEIRA). Otherwise, these two modes are mainly observed in solution by different techniques [41,42]. In SERS experiments, it is difficult to observe and distinguish these two vibrations modes because the EF will be potentially weak. Indeed, it is proportional to the extinction intensities (Q_e) [43,44], i.e. $EF \sim Q_e(\lambda_{exc}) \times Q_e(\lambda_{Raman})$. Therefore, $Q_e(\lambda_{Raman})$ or $Q_e(\lambda_{exc})$ will be weak because of the surface plasmon resonance position of the studied nanostructures and the great spectral redshift of λ_{Raman} with respect to λ_{exc} . In our case, SFG spectroscopy combines the advantages of selective LSPR excitation with intrinsic surface sensitivity, revealed by the specific phase shift parameter of this nonlinear optical technique.

5 Conclusion

In this paper, we employed honeycomb structured substrates of gold nanotriangles characterized by SFG spectroscopy in order to obtain an enhanced nonlinear optical signal from thiophenol molecules by using the excitation of localized surface plasmon resonance (transversal plasmon mode of gold nanotriangles deposited above a gold surface). In *ssp*-configuration, the excitation of this resonant transversal plasmon mode with the visible beam allowed to observe in SFG spectroscopy the ϵ and σ vibrational modes of thiophenol molecules localized close to the lateral sides of the gold triangles. In *ppp*-configuration, no peak is observed due to the strong *s-d* interband electronic transition of gold. Finally, SFG spectroscopy shows its relevance to be also used at the nanoscale on highly structured metallic SERS substrates. Indeed, SFG takes account of the surface gold electronic properties whatever their origin (plasmon, interband transition) affording complementary information on the molecular organisation and location on the surface of the nano-objects after chemical functionalization.

Conflict of interest

The authors declare that they have no conflicts of interests.

References

1. D. Lis and F. Cecchet. Localized surface plasmon resonances in nanostructures to enhance nonlinear vibrational spectroscopies: towards an astonishing molecular sensitivity. *Beilstein Journal of Nanotechnology*, 5:2275–2292, 2014.
2. M. Ben Haddada, M. Huebner, S. Casale, D. Knopp, R. Niessner, M. Salmann, and S. Boujday. Gold nanoparticles assembly on silicon and gold surfaces: Mechanism, stability, and efficiency in diclofenac biosensing. *The Journal of Physical Chemistry C*, 120(51):29302–29311, 2016.
3. H. B. de Aguiar, R. Scheu, K. C. Jena, A. G. F. de Beer, and S. Roke. Comparison of scattering and reflection SFG: a question of phase-matching. *Phys. Chem. Chem. Phys.*, 14:6826–6832, 2012.
4. X. Toledo-Fuentes, D. Lis, and F. Cecchet. Structural changes to lipid bilayers and their surrounding water upon interaction with functionalized gold nanoparticles. *The Journal of Physical Chemistry C*, 120(38):21399–21409, 2016.
5. C. Humbert and B. Busson. Chapter 10 - Sum-frequency generation spectroscopy of biointerfaces. In C.M. Pradier Y.J. Chabal, editor, *Biointerface Characterization by Advanced IR Spectroscopy*, pages 279 – 321. Elsevier, Amsterdam, 2011.
6. G. Barbillon. *Nanoplasmonics-Fundamentals and Applications*. InTech, Rijeka, 2017.
7. J. Yan, X. Han, J. He, L. Kang, B. Zhang, Y. Du, H. Zhao, C. Dong, H.-L. Wang, and P. Xu. Highly sensitive Surface-Enhanced Raman Spectroscopy (SERS) platforms based on silver nanostructures fabricated on polyaniline membrane surfaces. *ACS Applied Materials & Interfaces*, 4(5):2752–2756, 2012.
8. D. Jimenez de Aberasturi, A. B. Serrano-Montes, J. Langer, M. Henriksen-Lacey, W. J. Parak, and L. M. Liz-Marzn. Surface enhanced Raman scattering encoded gold nanostars for multiplexed cell discrimination. *Chemistry of Materials*, 28(18):6779–6790, 2016.
9. M. Sarkar, M. Besbes, J. Moreau, J.-F. Bryche, A. Olivéro, G. Barbillon, A.-L. Coutrot, B. Bartenlian, and M. Canva. Hybrid plasmonic mode by resonant coupling of localized plasmons to propagating plasmons in a Kretschmann configuration. *ACS Photonics*, 2(2):237–245, 2015.
10. G. Barbillon, V. E. Sandana, C. Humbert, B. Bélier, D. J. Rogers, F. H. Teherani, P. Bove, R. McClintock, and M. Razeghi. Study of Au coated ZnO nanoarrays for surface enhanced Raman scattering chemical sensing. *J. Mater. Chem. C*, 5:3528–3535, 2017.
11. J.-F. Bryche, R. Gillibert, G. Barbillon, M. Sarkar, A.-L. Coutrot, F. Hamouda, A. Aassime, J. Moreau, M. Lamy de la Chapelle, B. Bartenlian, and M. Canva. Density effect of gold nanodisks on the SERS intensity for a highly sensitive detection of chemical molecules. *Journal of Materials Science*, 50(20):6601–6607, 2015.
12. J.-F. Bryche, R. Gillibert, G. Barbillon, P. Gogol, J. Moreau, M. Lamy de la Chapelle, B. Bartenlian, and M. Canva. Plasmonic enhancement by a continuous gold underlayer: Application to SERS sensing. *Plasmonics*, 11(2):601–608, 2016.
13. D. Lis, Y. Caudano, M. Henry, S. Demoustier-Champagne, E. Ferain, and F. Cecchet. Selective plasmonic platforms based on nanopillars to enhance vibrational sum-frequency generation spectroscopy. *Advanced Optical Materials*, 1(3):244–255, 2013.

14. T. Kawai, D. J. Neivandt, and P. B. Davies. Sum frequency generation on surfactant-coated gold nanoparticles. *Journal of the American Chemical Society*, 122(48):12031–12032, 2000.
15. C. Humbert, O. Pluchery, E. Lacaze, A. Tadjeddine, and B. Busson. A multiscale description of molecular adsorption on gold nanoparticles by nonlinear optical spectroscopy. *Phys. Chem. Chem. Phys.*, 14:280–289, 2012.
16. O. Pluchery, C. Humbert, M. Valamanesh, E. Lacaze, and B. Busson. Enhanced detection of thiophenol adsorbed on gold nanoparticles by SFG and DFG nonlinear optical spectroscopy. *Phys. Chem. Chem. Phys.*, 11:7729–7737, 2009.
17. C. Humbert, B. Busson, J.-P. Abid, C. Six, H.H. Girault, and A. Tadjeddine. Self-assembled organic monolayers on gold nanoparticles: A study by sum-frequency generation combined with UV-Vis spectroscopy. *Electrochimica Acta*, 50(15):3101 – 3110, 2005.
18. G. Tourillon, L. Dreesen, C. Volcke, Y. Sartenaer, P. A. Thiry, and A. Peremans. Total internal reflection sum-frequency generation spectroscopy and dense gold nanoparticles monolayer: a route for probing adsorbed molecules. *Nanotechnology*, 18(41):415301, 2007.
19. G. Tourillon, L. Dreesen, C. Volcke, Y. Sartenaer, P. A. Thiry, and A. Peremans. Close-packed array of gold nanoparticles and sum frequency generation spectroscopy in total internal reflection: a platform for studying biomolecules and biosensors. *Journal of Materials Science*, 44(24):6805–6810, 2009.
20. C. Weeraman, A. K. Yatawara, A. N. Bordenyuk, and A. V. Benderskii. Effect of nanoscale geometry on molecular conformation: vibrational sum-frequency generation of alkanethiols on gold nanoparticles. *Journal of the American Chemical Society*, 128(44):14244–14245, 2006.
21. A. N. Bordenyuk, C. Weeraman, A. Yatawara, H. D. Jayatilake, I. Stioptkin, Y. Liu, and A. V. Benderskii. Vibrational sum frequency generation spectroscopy of dodecanethiol on metal nanoparticles. *The Journal of Physical Chemistry C*, 111(25):8925–8933, 2007.
22. L. Dalstein, M. Ben Haddada, G. Barbillon, C. Humbert, A. Tadjeddine, S. Boujday, and B. Busson. Revealing the interplay between adsorbed molecular layers and gold nanoparticles by linear and nonlinear optical properties. *The Journal of Physical Chemistry C*, 119(30):17146–17155, 2015.
23. C. Humbert, O. Pluchery, E. Lacaze, A. Tadjeddine, and B. Busson. Optical spectroscopy of functionalized gold nanoparticles assemblies as a function of the surface coverage. *Gold Bulletin*, 46(4):299–309, 2013.
24. J.-F. Bryche, A. Tsigara, B. Bélier, M. Lamy de la Chapelle, M. Canva, B. Bartenlian, and G. Barbillon. Surface enhanced Raman scattering improvement of gold triangular nanoprisms by a gold reflective underlayer for chemical sensing. *Sensors and Actuators B: Chemical*, 228:31 – 35, 2016.
25. A. Tsigara, A. Benkhial, S. Warren, F. Akkari, J. Wright, F. Frehill, and E. Dempsey. Metal microelectrode nanostructuring using nanosphere lithography and photolithography with optimization of the fabrication process. *Thin Solid Films*, 537:269 – 274, 2013.
26. C. L. Haynes and R. P. Van Duyne. Nanosphere lithography: a versatile nanofabrication tool for studies of size-dependent nanoparticle optics. *The Journal of Physical Chemistry B*, 105(24):5599–5611, 2001.
27. T. Hahn. *International Tables for Crystallography, Volume A: Space-group symmetry*. Springer, fifth ed. (corrected reprint), Dordrecht, 2005.
28. C.S. Tian and Y.R. Shen. Recent progress on sum-frequency spectroscopy. *Surface Science Reports*, 69(2):105 – 131, 2014.
29. C. Humbert, Y. Caudano, L. Dreesen, Y. Sartenaer, A.A. Mani, C. Silien, J.-J. Lemaire, P.A. Thiry, and A. Peremans. Self-assembled organic and fullerene monolayers characterisation by two-colour SFG spectroscopy: a pathway to meet doubly resonant SFG process. *Applied Surface Science*, 237(1-4):463 – 469, 2004.
30. A. Hohenau and J. R. Krenn. Plasmonic modes of gold nano-particle arrays on thin gold films. *Physica Status Solidi (RRL) Rapid Research Letters*, 4(10):256–258, 2010.
31. T. Feugmo, C. Giresse, and V. Liégeois. Analyzing the vibrational signatures of thiophenol adsorbed on small gold clusters by DFT calculations. *ChemPhysChem*, 14(8):1633–1645, 2013.
32. A. Tadjeddine, O. Pluchery, A. Le Rille, C. Humbert, M. Buck, A. Peremans, and W.-Q. Zheng. What can we learn from the non-linear optical investigation of the liquid–solid interface? *Journal of Electroanalytical Chemistry*, 473(1-2):25–33, 1999.
33. C. Humbert, L. Dreesen, A.A. Mani, Y. Caudano, J.-J. Lemaire, P.A. Thiry, and A. Peremans. IR-Visible sum-frequency vibrational spectroscopy of biphenyl-3 methylene thiol monolayer on gold and silver: effect of the visible wavelength on the SFG spectrum. *Surface Science*, 502-503(0):203 – 207, 2002.
34. L. Dreesen, C. Humbert, M. Celebi, J.J. Lemaire, A.A. Mani, P.A. Thiry, and A. Peremans. Influence of the metal electronic properties on the sum-frequency generation spectra of dodecanethiol self-assembled monolayers on Pt(111), Ag(111) and Au(111) single crystals. *Applied Physics B*, 74(7-8):621–625, 2002.
35. P. A. Covert and D. K. Hore. Assessing the gold standard: The complex vibrational nonlinear susceptibility of metals. *The Journal of Physical Chemistry C*, 119(1):271–276, 2015.
36. X. Zhuang, P. B. Miranda, D. Kim, and Y. R. Shen. Mapping molecular orientation and conformation at interfaces by surface nonlinear optics. *Phys. Rev. B*, 59:12632–12640, 1999.
37. B. Busson and A. Tadjeddine. Non-uniqueness of parameters extracted from resonant second-order nonlinear optical spectroscopies. *The Journal of Physical Chemistry C*, 113(52):21895–21902, 2009.
38. Y. R. Shen. *The principles of nonlinear optics*. John Wiley & Sons, Inc., 1984. 1st edition.
39. B. Bourguignon, W.-Q. Zheng, S. Carrez, A. Ouvrard, F. Fournier, and H. Dubost. Deriving the complete molecular conformation of self-assembled alkanethiol molecules from sum-frequency generation vibrational spectra. *Phys. Rev. B*, 79:125433, Mar 2009.
40. F. Cecchet, D. Lis, J. Guthmuller, B. Champagne, Y. Caudano, C. Silien, A. A. Mani, P. A. Thiry, and A. Peremans. Orientational analysis of dodecanethiol and p-Nitrothiophenol SAMs on metals with polarisation-dependent SFG spectroscopy. *ChemPhysChem*, 11(3):607–615, 2010.
41. L.-J. Wan, M. Terashima, H. Noda, and M. Osawa. Molecular orientation and ordered structure of benzenethiol adsorbed on gold(111). *The Journal of Physical Chemistry B*, 104(15):3563–3569, 2000.
42. S. Li, D. Wu, X. Xu, and R. Gu. Theoretical and experimental studies on the adsorption behavior of thiophenol on gold nanoparticles. *Journal of Raman Spectroscopy*, 38(11):1436–1443, 2007.

-
43. P. G. Etchegoin and E. C. Le Ru. *Surface enhanced Raman spectroscopy: Analytical, Biophysical and Life Science Applications*. Wiley, New York, 2011.
 44. G. Magno, B. Bélier, and G. Barbillon. Gold thickness impact on the enhancement of SERS detection in low-cost au/si nanosensors. *Journal of Materials Science*, 52(23):13650–13656, 2017.